Determine the Quantum Numbers of $X(6900)$ from Photon–Photon Fusion in Ultra-Peripheral Heavy Ion Collisions

Peng-Yu Niu(牛鹏宇)[1,2], Yan-Chun Ding(丁燕春)[1,2], Qian Wang(王倩)[1,2,3,4*], and Shuai Yang(杨帅)[1,2*]

[1]*State Key Laboratory of Nuclear Physics and Technology, Institute of Quantum Matter, South China Normal University, Guangzhou 510006, China*
[2]*Guangdong Basic Research Center of Excellence for Structure and Fundamental Interactions of Matter, Guangdong Provincial Key Laboratory of Nuclear Science, Guangzhou 510006, China*
[3]*Southern Center for Nuclear-Science Theory (SCNT), Institute of Modern Physics, Chinese Academy of Sciences, Huizhou 516000, China*
[4]*Research Center for Nuclear Physics (RCNP), Osaka University, Ibaraki 567-0047, Japan*

(Received 16 June 2025; accepted manuscript online 6 August 2025)

We study the production of the $X(6900)$ in the ultra-peripheral heavy ion collisions at the LHC energy region. The potential quantum numbers of $X(6900)$ could be $0^{\pm+}$ and $2^{\pm+}$. We find that the transverse momentum and the polar angle distributions of $X(6900)$ can be used to distinguish these four potential quantum numbers. These characteristic distributions originate from linearly polarized photons emitted by relativistic nuclei and can be measured by further LHC experiments.

DOI: 10.1088/0256-307X/42/10/100202 CSTR: 32039.14.0256-307X.42.10.100202

1. Introduction. Over the past two decades, tens of exotic states, which are not compatible with either $q\bar{q}$ or qqq configurations in the traditional quark model, have been discovered. Among them, an interesting exotic candidate is the fully heavy system, which was reported by the LHCb Collaboration in the J/ψ-pair invariant mass distribution[1,2] in pp collisions at center-of-mass energies of $\sqrt{s} = 7, 8, 13\,\text{TeV}$ with integrated luminosity of $9\,\text{fb}^{-1}$. A narrow structure around 6.9 GeV, named $X(6900)$, and a broad structure slightly above the $J/\psi J/\psi$ threshold was reported. Considering their mass positions and the observed channels, the community reached the consensus that they contain two charm quarks and two anti-charm quarks. Later on, the CMS Collaboration[3] reported three resonance-like structures through the same channel in pp collisions at $\sqrt{s} = 13\,\text{TeV}$ with an integrated luminosity of $135\,\text{fb}^{-1}$. The significances of the lower two structures with masses of $6927 \pm 9 \pm 5\,\text{MeV}$ and $6552 \pm 10 \pm 12\,\text{MeV}$ are larger than 5 standard deviations. The highest structure, with a mass of $7287 \pm 19 \pm 5\,\text{MeV}$, has a significance of 4.1 standard deviations. With higher statistics, all three structures are established with above 5σ.[4] The first one is consistent with $X(6900)$ reported by the LHCb Collaboration. Meanwhile, the ATLAS Collaboration[5] also reported similar structures. These structures are the first measurements of full-charm tetraquarks, arising intensive discussions among the hadron physics community.

The $X(6900)$ can be accepted by both compact tetraquark[6–20] and hadronic molecular pictures.[21–23] From the theoretical side, several potential options are proposed from various scenarios and the quantum number of $X(6900)$ is discussed. For the compact tetraquark picture, $X(6900)$ can be either a P-wave pseudoscalar with $J^{\text{PC}} = 0^{-+}$ [14] or an S-wave scalar with $J^{\text{PC}} = 0^{++}$.[24–30] Another possible quantum number of $X(6900)$ might be $J^{\text{PC}} = 2^{++}$ is also discussed in Refs. [6–9,27–33]. In the molecular picture, both $J^{\text{PC}} = 0^{++}$ and $J^{\text{PC}} = 2^{++}$ are allowed.[21,22] Therefore, determining its quantum numbers, especially distinguishing between 2^{++} and 0^{++}, would shed light on the nature of these recently measured full-charm tetraquark states. Recently, using angular analysis techniques, the CMS collaboration found that the quantum number of $X(6900)$ is most likely 2^{++}.[34]

To establish the quantum number of a given particle, the polarized beam is very useful. However, preparing the polarized beam is highly challenging in experiments. Alternatively, one may take advantage of the polarized photon in the ultra-peripheral collisions (UPC) process of heavy-ion collisions. The Lorentz-boosted electromagnetic fields surrounding ultrarelativistic heavy ions with large charges can be treated as a flux of quasireal photons.[35–37] The photon intensity is proportional to the square of the ion charge (Z). Exclusive photon–photon interactions, especially, the $\gamma\gamma \to l^+l^-$ processes, have been extensively studied both theoretically[38–50] and experimentally[51–57] in ultra-peripheral and hadronic heavy-ion collisions.

Moreover, photon–photon interactions can be used to study exotic particles,[58–63] Higgs bosons,[64–67] and to search for physics beyond the standard model.[68–71] Recently, people realized that the equivalent photon has impact parameter (b) dependence[57,72–75] and is linearly polarized.[76,77] Specifically, the linear polarized photons

*Corresponding authors. Email: qianwang@m.scnu.edu.cn; syang@scnu.edu.cn
© 2025 Chinese Physical Society and IOP Publishing Ltd. All rights, including for text and data mining, AI training, and similar technologies, are reserved.

lead to the $\cos(4\phi)$ azimuthal asymmetry for dilepton production from photon–photon scatterings, confirmed by the STAR Collaboration.[53] This linearly polarized quasireal photons could provide extra information about the spin of particle created by photon–photon fusion. In UPC, the nuclei pass on another with an impact parameter greater than twice the nuclear radius, which means that there is no overlap between the two nuclei. Based on these facts, UPC provides an excellent platform to investigate the quantum numbers of exotic states created by photon–photon fusion with the following advantages: (i) The background is significantly suppressed compared with that in hadronic collisions; (ii) The cross section is enhanced by Z^4 compared with that in e^+e^- collisions.

In this work, we focus on the kinematic distributions of $X(6900)$ to determine its quantum numbers (0^{++}, 0^{-+}, 2^{++}, or 2^{-+}), instead of the absolute cross section. We demonstrate that the kinematic distributions provide a powerful tool to identify its quantum numbers in future measurements at the LHC. This paper is organized as follows. Section 2 describes the details of the calculation. The results and discussions are presented in Section 3. Lastly, Section 4 provides a concluding summary.

2. Framework. The electromagnetic field surrounding ultra-relativistic nuclei is highly contracted and nearly perpendicular to the direction of motion, as depicted in Fig. 1. Therefore, the photons generated by these fields are expected to be linearly polarized in the transverse plane with respect to the beam.[76,77] The electromagnetic fields of the two nuclei are treated classically. The two nuclei are approximated to move with constant velocity on straight lines with an impact parameter b as shown in Fig. 2, with negligible deflections due to collision. The impact parameter b can be estimated using the event plane method, which is widely employed in elliptic flow measurements in heavy-ion collisions.[52,55,78–82] Meanwhile, photon–photon interactions remain the dominant process in peripheral heavy-ion collisions (60%–100% centrality) at transverse momenta below $P_{\rm T} \lesssim 150\,{\rm MeV}$.[52] From this point of view, our conclusions about the photon production of $X(6900)$ should still hold for the peripheral heavy-ion collisions. Accordingly, the two electromagnetic potentials are given by[72]

$$A_1^{\mu}(k_1, \boldsymbol{b}_1) = -2\pi Z_1 e \delta(k_1 \cdot u_1) \frac{F(-k_1^2)}{k_1^2} {\rm e}^{{\rm i}\boldsymbol{k}_1 \cdot \boldsymbol{b}_1} \times u_1^{\mu}, \quad (1)$$

$$A_2^{\mu}(k_2, \boldsymbol{b}_2) = -2\pi Z_2 e \delta(k_2 \cdot u_2) \frac{F(-k_2^2)}{k_2^2} {\rm e}^{{\rm i}\boldsymbol{k}_2 \cdot \boldsymbol{b}_2} \times u_2^{\mu}, \quad (2)$$

where the δ function ensures that the nuclei move along a straight line with constant velocity. k_1 and k_2 are the four momenta of the two photons, respectively. $u_1 = \gamma(1, 0, 0, -v)$ (Z_1) and $u_2 = \gamma(1, 0, 0, +v)$ (Z_2) are the four velocities (nuclear charge numbers) of the two nuclei, respectively. $\gamma = (1 - v^2)^{-1/2}$ is the Lorentz contraction factor. $\boldsymbol{b}_1 = (b, 0, 0)$ and $\boldsymbol{b}_2 = (0, 0, 0)$ are the coordinates of the two nuclei. $F(-k_1^2)$ and $F(-k_2^2)$ are the charge form

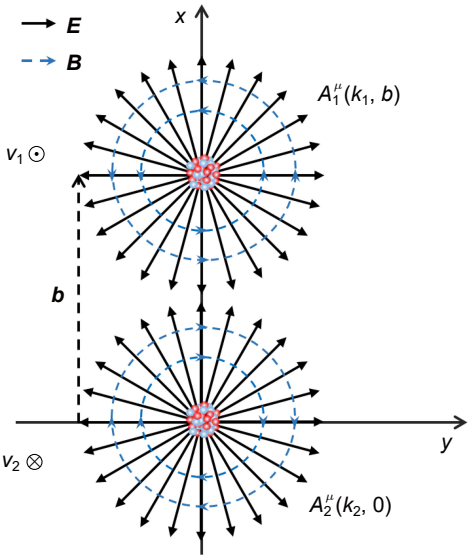

Fig. 1. Illustration of the electric and magnetic field lines in the plane perpendicular to the beam. The black solid and blue dashed lines represent the electric and magnetic fields, respectively. v_1 and v_2 are the velocities of the two nuclei in the center-of-mass frame. b is the impact parameter defined as the distance between the two nuclei in the transverse plane with respect to the beam.

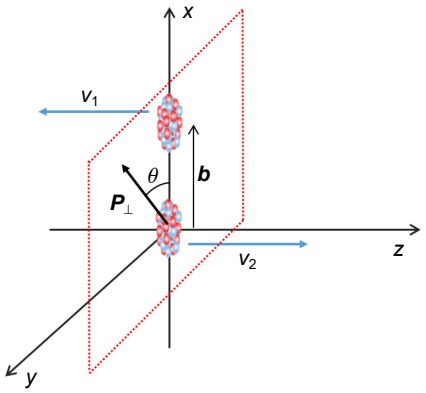

Fig. 2. The setup of the coordinate for the photon–photon fusion process in UPC. v_1 and v_2 are the velocities of two nuclei. The z-axis is chosen along beam direction. The direction of the nucleus–nucleus impact parameter $\boldsymbol{b}$ points from one nucleus to another, e.g., from nucleus with velocity v_2 to nucleus with velocity v_1, also serving as the direction of the x-axis. Thus, the y-axis can be determined by right hand rule.

factors of the two nuclei, which are the Fourier transforms of their spatial charge distribution,

$$F(k^2) = \int {\rm d}^3\boldsymbol{r} \rho(\boldsymbol{r}) {\rm e}^{{\rm i}\boldsymbol{k}\cdot\boldsymbol{r}}. \quad (3)$$

Here, $\boldsymbol{k}$ and $\boldsymbol{r}$ are momentum and coordinate, respectively. For a high-Z nucleus, the spatial charge distribution in the rest frame is well described by the Woods–Saxon distribution,[83]

$$\rho(r) = \frac{\rho_0}{1 + \exp[(r - R_A)/d]}, \quad (4)$$

where ρ_0 is the normalization factor. r is the distance

between a given point and the center of the nucleus. d and R_A are the skin depth and the radius of the nucleus, respectively. The employed values of those two parameters in this work are summarized in Table 1. However, it is hard to perform the Fourier transform analytically to obtain $F(k^2)$. Alternatively, an approximation

$$F(|k|) = \frac{4\pi\rho^0}{A|k^3|}\left(\frac{\sin(|k|R_A) - |k|R_A\cos(|k|R_A)}{1+a^2k^2}\right) \quad (5)$$

is widely employed.[84] Here A is the mass number of the nucleus and $R_A = 1.1A^{1/3}\,\text{fm}$ is the radius of Woods–Saxon distribution with a hard sphere[76] ($R_A = 1.2A^{1/3}\,\text{fm}$ is also used in Refs. [66,85]). a is the Yukawa potential range that is characterized by the inverse of the pion mass, i.e., 0.7 fm.[86] ρ_0 is also considered as a normalization factor, ensuring $F(0) = 1$.

A schematic diagram for the production of $X(6900)$ in the photon–photon fusion process is shown in Fig. 3. For the photon–photon fusion process, the nuclei can be assumed to move along straight line and their deflection can be neglected, as the transverse momentum is much smaller than the longitudinal momentum. Therefore, the emitted photon fields can be treated as electromagnetic external fields, and the production amplitude can be expressed as[72]

$$\begin{aligned}
&\mathcal{M}(k_1,k_2,P)\\
&= \int \frac{\mathrm{d}^4k_1}{(2\pi)^4}\frac{\mathrm{d}^4k_2}{(2\pi)^4}\left[A_1^\mu(k_1,b)\Gamma_{\mu\nu}(k_1,k_2)A_2^\nu(k_2,0)\right]\\
&\quad\times(2\pi)^4\delta^4(k_1+k_2-P)\\
&= Z^2\frac{e^2}{2v\gamma^2}\int\frac{\mathrm{d}^2\boldsymbol{k}_{1,\perp}}{(2\pi)^2}\frac{F(-k_1^2)}{-k_1^2}\frac{F(-k_2^2)}{-k_2^2}u_1^\mu u_2^\nu\Gamma_{\mu\nu}(k_1,k_2)\\
&\quad\times \mathrm{e}^{-\mathrm{i}\boldsymbol{b}\cdot\boldsymbol{k}_{1,\perp}}|_{k_2=P-k_1}, \qquad (6)
\end{aligned}$$

with $Z = Z_1 = Z_2$ and $F = F_1 = F_2$. Here, $\delta^4(k_1+k_2-P)$ is the requirement of the four momentum conservation. $P = (P_0, \boldsymbol{P}_\perp, P_z)$ is the four momentum of the produced particle. Here the subscript "$\perp$" is used to label the transverse component and the transverse momentum $\boldsymbol{P}_\perp = (P_x, P_y)$. $\Gamma_{\mu\nu}$ is the vertex function that depends on the quantum number of the produced particle and will be discussed in details later. The two photon momenta k_1 and k_2 read

$$k_1 = (\omega_1, \boldsymbol{k}_\perp, \omega_1/v), \quad k_2 = (\omega_2, \boldsymbol{P}_\perp - \boldsymbol{k}_\perp, -\omega_2/v), \quad (7)$$

with $\omega_1 = 1/2(P_0 + vP_z)$ and $\omega_2 = 1/2(P_0 - vP_z)$ the energies of the 1st and 2nd photons, respectively. Because the transverse momentum is much smaller than the longitudinal momentum, the two photons can be approximately on-shell. Considering that $|\boldsymbol{k}_\perp|_{\min} = 0$, one obtains

$$k_1^2 = \omega_1^2 - \boldsymbol{k}_{1\perp}^2 - \omega_1^2/v^2 \le \omega_1^2 - \omega_1^2/v^2 \approx -\left(\frac{\omega_1}{\gamma}\right)^2. \quad (8)$$

In the last step, $v \approx 1$ is used.

Table 1. The employed values of the skin depth d and the radius R_A of Au and Pb.

Refs.	Ref. [88]		Ref. [73,76]	
Nucleus	Au	Pb	Au	Pb
d [fm]	0.41	0.45	0.535	0.546
R_A [fm]	6.42	6.66	6.38	6.62

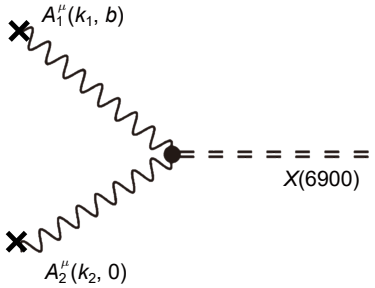

Fig. 3. The schematic diagram for the production of the $X(6900)$ with two classical external fields $A_{1,2}^\mu$.

In e^+e^- collisions, the deflection of the scattering electron or positron leads to finite virtuality of the emitted photon. In contrast, heavy ions maintain a straight-line trajectory in UPC. Thus, the low-energy photon is regulated by the finite Lorentz contraction factor γ of the ions, i.e., $|k^2| \ge (\omega/\gamma)^2$, with ω being the photon energy. The high-energy photon is naturally cut off by the finite size of the ion's charge distribution, i.e., $|k^2| \le (1/R_A)^2$, in which R_A is the nuclear radius.[72] These are consistent with Eq. (8). For a given nucleus, the transverse momentum of the photon is constrained by $k_\perp^2 \le 1/R_A^2 - (\omega/\gamma)^2$.

In this paper, we consider the production of hadrons with all the possible quantum numbers, i.e., $0^{\pm+}$ and $2^{\pm+}$, in the photon–photon fusion process. Hadrons with spin-1 cannot be produced due to the Landau–Yang theorem.[89] For scalars[72] and pseudoscalars, the vertex functions are

$$\Gamma_{\mu\nu}^{0^{++}} = g_s(k_1\cdot k_2 g_{\mu\nu} - k_{1\nu}k_{2\mu}), \quad (9)$$

$$\Gamma_{\mu\nu}^{0^{-+}} = g_{sp}\epsilon_{\mu\nu\alpha\beta}k_1^\alpha k_2^\beta, \quad (10)$$

respectively. k_1 and k_2 are four momenta of the two photons. g_s and g_{sp} are the corresponding effective couplings. The vertex functions for $2^{\pm+}$ hadrons can be built with the covariant tensor formalism[90] as

$$\begin{aligned}
\Gamma_{\mu\nu}^{2^{++}} &= g_t(g_{\mu\nu}k_{1\rho}k_{2\sigma}\epsilon^{\rho\sigma} + k_1\cdot k_2\epsilon^{\mu\nu}\\
&\quad - k_{1\mu}k_{2\rho}\epsilon^{\rho\nu} - k_{2\mu}k_{1\rho}\epsilon^{\rho\nu}), \qquad (11)\\
\Gamma_{\mu\nu}^{2^{-+}} &= g_{tp}\epsilon_{\mu\lambda\alpha\beta}k_1^\alpha k_2^\beta\epsilon_\nu^\lambda. \qquad (12)
\end{aligned}$$

The polarized vector of the spin-2 particles reads[91]

$$\epsilon_{\mu\nu}(\boldsymbol{p},\lambda) = \sum_{\lambda_1,\lambda_2}\langle 1,\lambda_1;1,\lambda_2|2,\lambda\rangle\epsilon_\mu(\boldsymbol{p},\lambda_1)\epsilon_\nu(\boldsymbol{p},\lambda_2) \quad (13)$$

with λ indicating the third component of spin. $\boldsymbol{p}$ is the three momentum of the produced tensor. If the vertex function $\Gamma_{\mu\nu}$ contracts with two real photons, it is easy to verify that the amplitudes satisfy gauge invariance.

With the above amplitudes, one can obtain the differential cross section[72]

$$\mathrm{d}\sigma = \mathrm{d}^2\boldsymbol{b}|\mathcal{M}(k_1,k_2,P)|^2\frac{\mathrm{d}^4P}{(2\pi)^4}\mathrm{d}\alpha, \quad (14)$$

where $\mathrm{d}\alpha$ is the n-body phase space,

$$\mathrm{d}\alpha = \delta^4\left(P - \sum_{i=1}^{n} p_i\right)\frac{\mathrm{d}^3\boldsymbol{p}_1}{(2\pi)^3 2E_1} \times \frac{\mathrm{d}^3\boldsymbol{p}_2}{(2\pi)^3 2E_2}\cdots\frac{\mathrm{d}^3\boldsymbol{p}_n}{(2\pi)^3 2E_n}. \quad (15)$$

In this paper, only one-body phase space should be considered. Thus, the differential cross section can be simplified to the following form:

$$\sigma = \frac{2}{(2\pi)^3 2|P_z|}\int \mathrm{d}^2\boldsymbol{b}|\mathcal{M}(k_1,k_2,P)|^2\mathrm{d}P_0 \times \mathrm{d}^2\boldsymbol{P}_\perp\theta(E_0)|_{P_z=\sqrt{P_0^2-\boldsymbol{P}_\perp^2-M_X^2}}, \quad (16)$$

where M_X is the mass of the hadron $X(6900)$. As the effective couplings g_s, g_{sp}, g_t, and g_{tp} are not determined, the total cross section cannot be accurately predicted. The production cross section of $X(6900)$ in the photon–photon fusion process has been estimated by the vector meson dominance model in Ref. [63]. Our work focuses on the transverse momentum $\boldsymbol{P}_\perp$ distribution $\mathrm{d}\sigma/(\mathrm{d}\boldsymbol{P}_\perp)$ and the polar angle distribution $\mathrm{d}\sigma/(\mathrm{d}\theta)$ of $X(6900)$, which can be used to distinguish various quantum numbers. These two distributions can be obtained by integrating out another dimension from

$$\frac{\mathrm{d}\sigma}{\mathrm{d}|\boldsymbol{P}_\perp|\,\mathrm{d}\theta} \propto \int \mathrm{d}^2\boldsymbol{b}\mathrm{d}P_0|\boldsymbol{P}_\perp|\,|\mathcal{M}(k_1,k_2,P)|^2|_{P_z=\sqrt{P_0^2-\boldsymbol{P}_\perp^2-M_X^2}}, \quad (17)$$

where θ is the azimuth angle of $\boldsymbol{P}_\perp$ as illustrated in Fig. 2. Because that the value of the total transverse momentum $\boldsymbol{P}_\perp$ is small in UPC, P_z is treated as a constant number in the last step.

3. Results and Discussions. The collision time of the UPC is about $t_{\rm coll} = R_A/\gamma$, and the maximum energy of the photon is about $\omega_{\rm max} \approx \gamma/R_A$ [72] due to the uncertainty principle. Taking the Pb beam with the energy per nucleon $\sqrt{s_{\rm NN}} = 5.628\,\mathrm{TeV}$ as an example, the maximum photon energy can reach $\sim 90\,\mathrm{GeV}$ with $\gamma = 3000$ and $R_A = 6\,\mathrm{fm}$.[50] Such a large energy can produce hadron with a mass as large as $X(6900)$ as discussed in Section 1. The production of $X(6900)$ has been studied in heavy ion collision.[62,63] In principle, the photon energy should be integrated out to estimate the cross section of $X(6900)$. However, we have checked that the transverse momentum $\boldsymbol{P}_\perp$ and the polar angle θ distributions, which essentially help to pin down the quantum numbers of the interested hadrons, are not sensitive to the two-photon center-of-mass energy $\sqrt{s_{\gamma\gamma}}$ in UPC (hereafter $\sqrt{s_{\gamma\gamma}}$ will be abbreviated as $\sqrt{s}$). As a result, in this work, $\sqrt{s}$ is set to 20 GeV as an illustration. The lower limit and upper limit of the impact parameter $b = |\boldsymbol{b}|$ are twice nuclei radius and $+\infty$, respectively. Since the cross section decreases dramatically with the increasing b,[72] the upper limit of the impact parameter b is set to 200 fm. We have checked that when this value increases to 300 fm and 400 fm, our results do not change. In addition, the upper limit of $|\boldsymbol{k}_{1\perp}|$ is set to 0.05 GeV which is larger than the value used in Refs. [50,72,85]. With all the parameter constraints imposed, we can obtain the $\boldsymbol{P}_\perp$ and θ distributions from Eq. (17) for all possible quantum numbers, i.e., $J^{\rm PC} = 0^{\pm+}$ and $J^{\rm PC} = 2^{\pm+}$.

The differential cross sections $\frac{\mathrm{d}\sigma}{\mathrm{d}P_\perp}$ and $\frac{\mathrm{d}\sigma}{P_\perp\mathrm{d}P_\perp}$, with polar angle θ and impact parameter b integrated out, are presented in Fig. 4. In Fig. 4(b), the states with negative parity go to zero faster than those with positive parity around $P_\perp = 0$. That is because the antisymmetric tensor in the vertex function for the states with negative parity contracts with the photon momenta and the polarization vector/tensor of a given state. When $P_\perp = 0$, $\boldsymbol{k}_{1\perp}$ and $\boldsymbol{k}_{2\perp}$ are symmetric, i.e., $\boldsymbol{k}_{1\perp} = -\boldsymbol{k}_{2\perp}$, and the amplitudes of the 0^- and 2^- states obviously go to zero. That is the reason why the $P_\perp$ distributions with negative parity go to zero faster than those with positive parity. This can be used to distinguish different parities. One can also see in Fig. 4 that the $P_\perp$ distributions of the states with the same parity have similar behavior, which is because of the similar structure of the vertex function. While the four curves also share the same characteristic that the differential cross section decreases with increasing $P_\perp$.

We borrow the idea from the oscillation behavior of the dilepton pair distribution in UPC[76,77,92] and also present

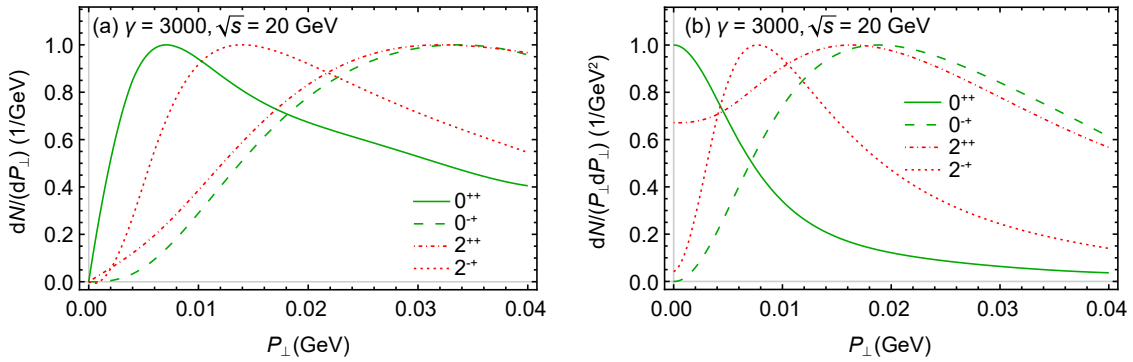

Fig. 4. The differential $\frac{\mathrm{d}\sigma}{\mathrm{d}P_\perp}$ (panel a) and $\frac{\mathrm{d}\sigma}{P_\perp\mathrm{d}P_\perp}$ (panel b) distributions with polar angle θ and the impact parameter b integrated out. As all the effective couplings g_s, g_{sp}, g_t, and g_{tp} are not determined, all the curves are rescaled to make the largest value to be one. The green solid and green dashed curves are for the 0^{++} and 0^{-+} states, respectively. The red dot-dashed and the red dotted curves are for the 2^{++} and 2^{-+} states, respectively.

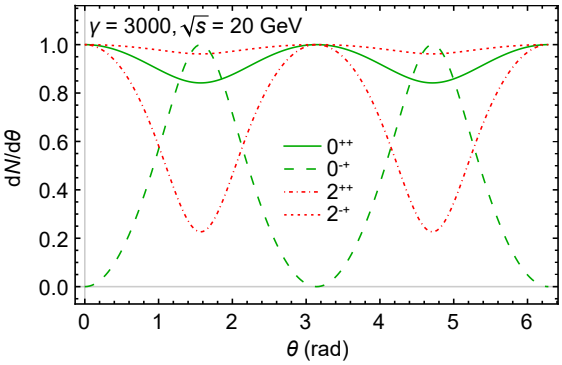

Fig. 5. The differential polar angle θ distributions with the transverse momentum $\boldsymbol{P}_\perp$ and the impact parameter b integrated out. All the curves are also rescaled to make their large values to be one. The labels are analogous to those in Fig. 4.

the differential polar angle θ distributions in Fig. 5. They oscillate with the period π for all cases. There is no doubt that the system is symmetric with respect to the plane in which the two heavy ions locate, i.e., the xz plane in Fig. 2. The 0^+, 2^+, and 2^- distributions are "W"-type and the 0^- distribution is "M"-type. This can be used to distinguish the 0^- quantum number from the others. The oscillation strengths of the 0^- and 2^+ states are larger than those of the other two scenarios.

Figure 6 shows the differential polar angle θ distributions for the transverse momentum regions $(0.00, 0.01]$, $(0.01, 0.02]$, $(0.02, 0.03]$, $(0.03, 0.04]$, and $(0.04, 0.05]$ GeV. The 0^{-+} and 2^{++} states oscillate more significantly than the 0^{++} and 2^{-+} states, which can be seen in Fig. 5. The 0^{-+} distributions for all the $P_\perp$ regions are "M" type, and the distributions for other states for all the $P_\perp$ regions are "W" type. The oscillation for the 2^{++} state is more significant than that of the 0^{++} and 2^{-+} states. The largest values of the 0^{++} and 2^{-+} states are the $(0.00, 0.01]$ GeV and $(0.01, 0.02]$ GeV regions, respectively. This behavior can be used to distinguish these two states.

The above distributions, which could be measured at the LHC, can be used to determine the quantum numbers of $X(6900)$. As our framework does not depend on the property of $X(6900)$, it cannot help to shed light on its internal structure, for instance, compact tetraquark or hadronic molecule. It also means that our framework works not only for $X(6900)$, but also for other regular and exotic hadrons.

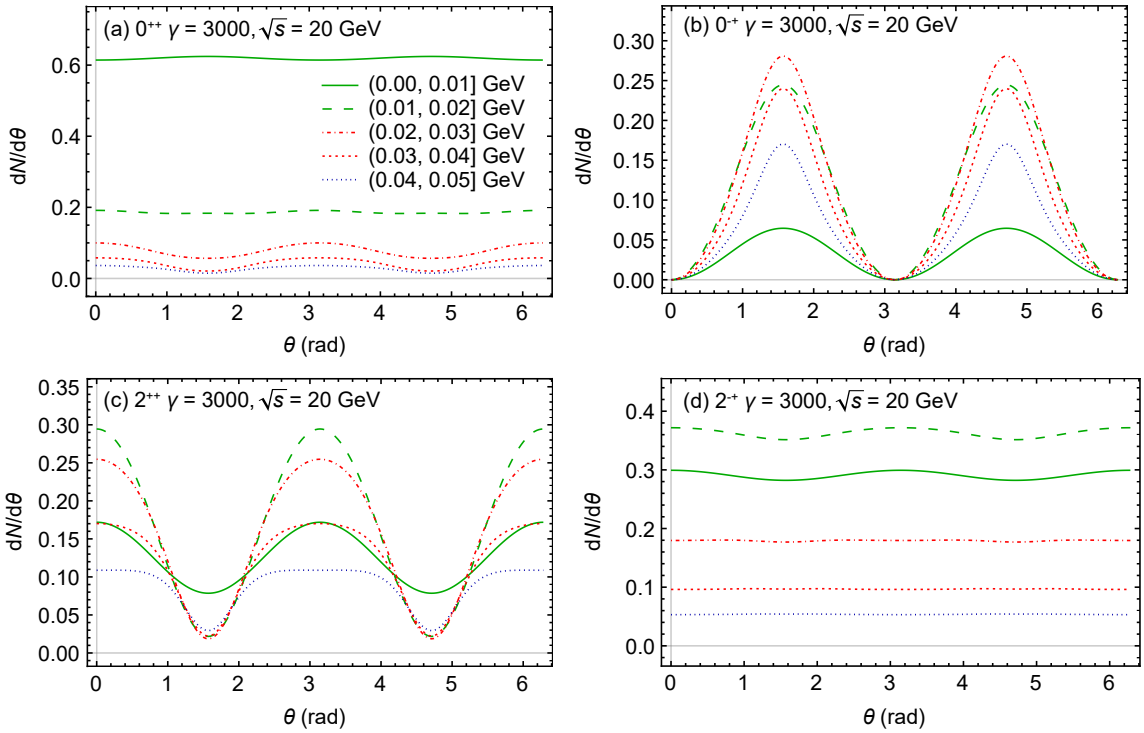

Fig. 6. The differential polar angle θ distributions for various transverse momentum regions with the Lorentz contraction parameters $\gamma = 3000$ and the two-photon center-of-mass energy $\sqrt{s} = 20$ GeV. The green solid, green long dashed, red dot-dashed, red dashed, and blue dotted curves are used to label the distributions of the transverse momentum regions $(0.00, 0.01]$,$(0.01, 0.02]$, $(0.02, 0.03]$,$(0.03, 0.04]$, and $(0.04, 0.05]$ GeV, respectively.

4. Summary. Since the observation of the first full-charm tetraquark $X(6900)$, the community has intensively discussed its internal structure, i.e., either compact tetraquark or hadronic molecule. For the compact tetraquark scenario, all $J^{\rm PC} = 0^{\pm+}$ and $2^{\pm+}$ quantum numbers are allowed. However, its quantum numbers cannot be well established due to the low statistics in current experiments. We take advantage of the polarized photons produced in the UPC and predict the transverse momentum and polar angle distributions of $X(6900)$. These two distributions exhibit significant differences for the four potential quantum numbers $J^{\rm PC} = 0^{\pm+}$, $2^{\pm+}$, which can be

used to help determine the quantum number of $X(6900)$. As this method does not depend on the internal structure of the hadrons, it can also work for other hadrons with spin other than one.

Acknowledgements. The discussion with Wangmei Zha and Hui Zhang is acknowledged. This work was partly supported by the Guangdong Major Project of Basic and Applied Basic Research (Grant Nos. 2020B0301030008 and 2023A1515010416), and the National Natural Science Foundation of China (Grant Nos. 12375073, 12275091, 12147128, and 12035007).

References

[1] Aaij R, Adeva B, Adinolfi M *et al.* (LHCb) 2018 *JHEP* **2018** 086
[2] Aaij R, Beteta C A, Ackernley T *et al.* (LHCb) 2020 *Sci. Bull.* **65** 1983
[3] The CMS Collaboration CMS-PAS-BPH-21-003
[4] The CMS Collaboration CMS-PAS-BPH-24-003
[5] The ATLAS Collaboration ATLAS-CONF-2022-040
[6] Faustov R N, Galkin V O, and Savchenko E M 2021 *Universe* **7** 94
[7] Deng C R, Chen H, and Ping J L 2021 *Phys. Rev. D* **103** 014001
[8] Chen H X, Chen W, Liu X, Liu Y R, and Zhu S L 2023 *Rept. Prog. Phys.* **86** 026201
[9] Weng X Z, Chen X L, Deng W Z, and Zhu S L 2021 *Phys. Rev. D* **103** 034001
[10] Richard J M 2020 *Sci. Bull.* **65** 1954
[11] Sonnenschein J and Weissman D 2021 *Eur. Phys. J. C* **81** 25
[12] Guo Z H and Oller J A 2021 *Phys. Rev. D* **103** 034024
[13] Berezhnoy A V, Luchinsky A V, and Novoselov A A 2012 *Phys. Rev. D* **86** 034004
[14] Wu J, Liu Y R, Chen K, Liu X, and Zhu S L 2018 *Phys. Rev. D* **97** 094015
[15] Chen X Y 2010 arXiv:2001.06755 [hep-ph]
[16] Liu M S, Lü Q F, Zhong X H, and Zhao Q 2019 *Phys. Rev. D* **100** 016006
[17] Wang G J, Meng L, and Zhu S L 2019 *Phys. Rev. D* **100** 096013
[18] Zhao Z, Xu K, Kaewsnod A, Liu X Y, Limphirat A, and Yan Y P 2021 *Phys. Rev. D* **103** 116027
[19] Chen H X, Chen W, Liu X, and Zhu S L 2020 *Sci. Bull.* **65** 1994
[20] Wang Z G 2020 *Chin. Phys. C* **44** 113106
[21] Dong X K, Baru V, Guo F K, Hanhart C, Nefediev A, and Zou B S 2021 *Sci. Bull.* **66** 2462
[22] Dong X K, Baru V, Guo F K, Hanhart C, and Nefediev A 2021 *Phys. Rev. Lett.* **126** 132001 Erratum: [2022 *Phys. Rev. Lett.* **127** 119901]
[23] Wang J Z and Liu X 2022 *Phys. Rev. D* **106** 054015
[24] Debastiani V R and Navarra F S 2019 *Chin. Phys. C* **43** 013105
[25] Liu M S, Liu F X, Zhong X H, and Zhao Q 2024 *Phys. Rev. D* **109** 076017
[26] Wan B D and Qiao C F 2021 *Phys. Lett. B* **817** 136339
[27] Karliner M and Rosner J L 2020 *Phys. Rev. D* **102** 114039
[28] Lü Q F, Chen D Y, and Dong Y B 2020 *Eur. Phys. J. C* **80** 871
[29] Li Q, Chang C H, Wang G L, and Wang T H 2021 *Phys. Rev. D* **104** 014018
[30] Ke H W, Han X, Liu X H, and Shi Y L 2021 *Eur. Phys. J. C* **81** 427
[31] Liang Z R, Wu X Y, and Yao D L 2021 *Phys. Rev. D* **104** 034034
[32] Bedolla M A, Ferretti J, Roberts C D, and Santopinto E 2020 *Eur. Phys. J. C* **80** 1004
[33] Zhu R L 2021 *Nucl. Phys. B* **966** 115393
[34] The CMS Collaboration CMS-PAS-BPH-24-002
[35] Fermi E 1924 *Z. Phys.* **29** 315
[36] Williams E J 1934 *Phys. Rev.* **45** 729
[37] von Weizsacker C F 1934 *Z. Phys.* **88** 612
[38] Budnev V M, Ginzburg I F, Meledin G V, and Serbo V G 1975 *Phys. Rept.* **15** 181
[39] Bertulani C A and Baur G 1988 *Phys. Rept.* **163** 299
[40] Baur G, Hencken K, Trautmann D, Sadovsky S, and Kharlov Y 2002 *Phys. Rept.* **364** 359
[41] Bertulani C A, Klein S R, and Nystrand J 2005 *Ann. Rev. Nucl. Part. Sci.* **55** 271
[42] Baur G, Hencken K, and Trautmann D 2007 *Phys. Rept.* **453** 1
[43] Baltz A J, Baur G, d'Enterria D *et al.* 2008 *Phys. Rept.* **458** 1
[44] Klein S and Steinberg P 2020 *Ann. Rev. Nucl. Part. Sci.* **70** 323
[45] Zha W M, Ruan L J, Tang Z B, Xu Z J, and Yang S 2018 *Phys. Lett. B* **781** 182
[46] Klein S R 2018 *Phys. Rev. C* **97** 054903
[47] Azevedo C, Gonçalves V P, and Moreira B D 2019 *Eur. Phys. J. C* **79** 432
[48] Klein S, Mueller A H, Xiao B W, and Yuan F 2020 *Phys. Rev. D* **102** 094013
[49] Xiao B W, Yuan F, and Zhou J 2020 *Phys. Rev. Lett.* **125** 232301
[50] Brandenburg J D, Zha W M, and Xu Z B 2021 *Eur. Phys. J. A* **57** 299
[51] Adams J, Aggarwal M M, Ahammed Z *et al.* (STAR) 2004 *Phys. Rev. C* **70** 031902
[52] Adam J, Adamczyk L, Adams J *et al.* (STAR) 2018 *Phys. Rev. Lett.* **121** 132301
[53] Adam J, Adamczyk L, Adams J *et al.* (STAR) 2021 *Phys. Rev. Lett.* **127** 052302
[54] Abbas E, AbelevB, Adam J *et al.* (ALICE) 2013 *Eur. Phys. J. C* **73** 2617
[55] Aaboud M, Aad G, Abbott B *et al.* (ALICE) 2018 *Phys. Rev. Lett.* **121** 212301
[56] Aad G, Abbott B K, Abbott B *et al.* (ALICE) 2021 *Phys. Rev. C* **104** 024906
[57] Sirunyan A M, Tumasyan A, Adam W *et al.* (CMS) 2021 *Phys. Rev. Lett.* **127** 122001
[58] Goncalves V P, da Silva D T, and Sauter W K 2013 *Phys. Rev. C* **87** 028201
[59] Gonçalves V P and Jaime M W 2020 *Phys. Lett. B* **805** 135447
[60] Moreira B D, Bertulani C A, Goncalves V P, and Navarra F S 2016 *Phys. Rev. D* **94** 094024
[61] Goncalves V P and Moreira B D 2019 *Eur. Phys. J. C* **9** 7
[62] Gonçalves V P and Moreira B D 2021 *Phys. Lett. B* **816** 136249
[63] Esposito A, Manzari C A, Pilloni A, and Polosa A D 2021 *Phys. Rev. D* **104** 114029
[64] Drees M, Ellis J R, and Zeppenfeld D 1989 *Phys. Lett. B* **223** 454
[65] Papageorgiu E 1990 *Phys. Lett. B* **250** 155
[66] Zhu J Q, Ma Z L, Shi C Y, and Li Y D 2015 *Nucl. Phys. B* **900** 431
[67] d'Enterria D, Martins D E, and Rebello Teles P 2020 *Phys. Rev. D* **101** 033009
[68] Bruce R, d'Enterria D, de Roeck A *et al.* 2020 *J. Phys. G* **47** 060501
[69] Aaboud M, Aad G, Abbott B *et al.* (ATLAS) 2017 *Nature Phys.* **13** 852
[70] Aad G, Abbott B, Abbott D C *et al.* (ATLAS) 2021 *JHEP* **2021** 050

[71] Sirunyan A M, Tumasyan A, Adam W *et al.* (CMS) 2019 *Phys. Lett. B* **797** 134826
[72] Vidovic M, Greiner M, Best C, and Soff G 1993 *Phys. Rev. C* **47** 2308
[73] Zha W M, Brandenburg J D, Tang Z B, and Xu Z B 2020 *Phys. Lett. B* **800** 135089
[74] Wang R J, Pu S, and Wang Q 2021 *Phys. Rev. D* **104** 056011
[75] Kłusek-Gawenda M, Schäfer W, and Szczurek A 2021 *Phys. Lett. B* **814** 136114
[76] Li C, Zhou J, and Zhou Y J 2019 *Phys. Lett. B* **795** 576
[77] Li C, Zhou J, and Zhou Y J 2020 *Phys. Rev. D* **101** 034015
[78] Abdallah M, Aboona B, Adam J *et al.* (STAR) 2022 *Phys. Rev. C* **105** 064911
[79] Chatrchyan S, Khachatryan V, Sirunyan A M *et al.* (CMS) 2013 *Phys. Rev. Lett.* **109** 022301
[80] Ackermann K H, Adams N, Adler C *et al.* (STAR) 2001 *Phys. Rev. Lett.* **86** 402
[81] Adare A, Aidala C, Ajitanand N N *et al.* (PHENIX) 2018 *Phys. Rev. Lett.* **121** 222301
[82] Adam J, Adamczyk L, Adams J R *et al.* (STAR) 2019 *Phys. Rev. Lett.* **123** 132302
[83] Woods R D and Saxon D S 1964 *Phys. Rev.* **95** 577
[84] Klein S and Nystrand J 1999 *Phys. Rev. C* **60** 014903
[85] Baur G, Hencken K, and Trautmann D 1998 *J. Phys. G* **24** 1657
[86] Davies K T R and Nix J R 1976 *Phys. Rev. C* **14** 1977
[87] De Vries H, De Jager C W, and De Vries C 1987 *Atom. Data Nucl. Data Tabl.* **36** 495
[88] Shou Q Y, Ma Y G, Sorensen P, Tang A H, Videbæk F, and Wang H H 2015 *Phys. Lett. B* **749** 215
[89] Yang C N 1950 *Phys. Rev.* **77** 242
[90] Zou B S and Bugg D V 2003 *Eur. Phys. J. A* **16** 537
[91] Zou B S and Hussain F 2023 *Phys. Rev. C* **67** 015204
[92] Klein S R, Nystrand J, Seger J, Gorbunov Y, and Butterworth J 2017 *Comput. Phys. Commun.* **212** 258